Investigating New Reactivities Enabled by Polariton Photochemistry

Arkajit Mandal and Pengfei Huo*

Department of Chemistry, University of Rochester, 120 Trustee Road, Rochester, New York 14627, United States

E-mail: pengfei.huo@rochester.edu

Model System

In this section, we provide detailed expressions of the model Hamiltonian used in this study, as well as the bath descritization procedure.

The electronic Hamiltonian $\hat{H}_{\mathrm{e}}$ is described by a model system that undergoes isomerization reaction[1]

$$\hat{H}_e = \hat{T}_R + E_g(R)|g\rangle\langle g| + E_e(R)|e\rangle\langle e|. \tag{S1}$$

Here, $|\alpha\rangle \in \{|g\rangle, |e\rangle\}$ represents the electronic ground or excited state, R represents the reaction coordinate, $\hat{T}_R$ is the nuclear kinetic energy operator.

The electronic potential $E_g(R)$ and $E_e(R)$ are modeled with the following expression

$$\begin{aligned} E_g(R) &= \frac{v_1(R) + v_2(R)}{2} - \sqrt{D_1^2 + \frac{(v_1(R) - v_2(R))^2}{4}} \\ E_e(R) &= \frac{v_3(R) + v_4(R)}{2} - \sqrt{D_2^2 + \frac{(v_3(R) - v_4(R))^2}{4}} \end{aligned} \tag{S2}$$

where $v_i(R) = A_i + B_i(R - R_i)^2$, and the rest of the parameters (in a.u.) are tabulated below

i	A_i	B_i	R_i	D_i
1	0.049244	0.18	-0.75	0.073
2	0.010657	0.18	0.85	0.514
3	0.428129	0.18	-1.15	-
4	0.373005	0.147	1.25	-

To clearly demonstrate the effect from quantum light-matter interaction, we choose to not include the non-adiabatic coupling $\langle g|\nabla_R|e\rangle$ in our model system. With this assumption, both $|g\rangle$ and $|e\rangle$ states effectively become diabatic states.

The reaction coordinate R is coupled to the other vibrational modes $\mathbf{r} = \{r_k\}$ in the molecule, modeled by the system-bath Hamiltonian $\hat{H}_{\rm sb}$ as follows

$$\hat{H}_{\rm sb} = \hat{T}_{\mathbf{r}} + \sum_k \frac{1}{2}\omega_k^2 \left[r_k + \frac{c_k R}{\omega_k^2} \right]^2. \tag{S3}$$

In the above equation, $\hat{T}_{\mathbf{r}}$ represents the kinetic energy of the phonon modes, r_k is the $k_{\rm th}$ phonon mode with the corresponding coupling constant c_k and frequency ω_k.

The dissipative bath has the following Ohmic spectral density

$$J(\omega) = \frac{\pi}{2} \sum_{k=1}^{N} \frac{c_k^2}{\omega_k} \delta(\omega - \omega_k) = \frac{1}{2} \pi \xi \omega e^{-\omega/\omega_b}, \tag{S4}$$

where $\xi = 12$ is the Kondo parameter and $\omega_b = 1324.02$ cm^{-1} is the characteristic frequency[2,3] of the phonon bath, which is typical for molecualr vibrations. The corresponding reorganization energy is $\lambda = \frac{1}{\pi}\int_0^\infty d\omega J(\omega)/\omega = 22.7$ kcal/mol. To sample the spectral density with a set of discretized mode, we use the following scheme[2]

$$\omega_k = -\omega_b \ln \left[1 - k \frac{1 - e^{-\omega_m/\omega_b}}{N} \right] \tag{S5}$$

$$c_k = \sqrt{\frac{\xi \omega_b (1 - e^{-\omega_m/\omega_b})}{N}} \omega_k. \tag{S6}$$

Here, $\omega_m = 4\omega_b$ is a numerical cutoff of the frequency, and $N = 800$ is the number of phonon bath modes used to discretize the spectral density.

PLDM quantum dynamics approach

In this work, we apply Partial Linearized Density Matrix Dynamics (PLDM) path-integral dynamic method to perform quantum dynamics calculations.[4]

We begin by expressing the total Hamiltonian as $\hat{H} = \hat{T}+\hat{V}_0+\hat{V} \equiv \hat{T}+\hat{V}_0+\sum_{ij} V_{\mu\nu}(\mathbf{R})|i\rangle\langle j|$. Here, $|i\rangle$ is the strict diabatic basis. For our light-matter interaction Hamiltonian in this study, $|i\rangle \in \{|g,1\rangle, |e,0\rangle\}$ for the single molecule case, and in the two molecule case $|i\rangle \in \{|\alpha_1, \beta_2, n\rangle\}$, where $\{|\alpha_1\rangle, |\beta_2\rangle\} \in \{|g\rangle, |e\rangle\}$. Further, $\hat{T} = \hat{T}_R + \hat{T}_{\mathbf{r}}$ is the kinetic energy operator for nuclear degrees of freedom, and $\hat{V}_0 = \hat{H}_{\mathrm{sb}} - \hat{T}_{\mathbf{r}}$ is the state-independent system-bath potential.

In the PLDM path-integral approach, we use the mapping representation of Meyer-Miller-Stock-Thoss[5–7] to transform the discrete electronic states into continuous variables $|i\rangle\langle j| \to \hat{b}_i^\dagger \hat{b}_j$, where $\hat{b}_i^\dagger = \frac{1}{\sqrt{2\hbar}}(\hat{q}_i - \mathrm{i}\hat{p}_i)$ and $\hat{b}_j = \frac{1}{\sqrt{2\hbar}}(\hat{q}_j + \mathrm{i}\hat{p}_j)$. Applying a linearization approximation[4] to the nuclear degrees of freedom and keeping the explicit propagation of the electronic degrees of freedom, we arrive at the PLDM expression for computing reduced density matrix[4,8]

$$\rho_{ij}(t) = \mathrm{Tr}_{\mathrm{R},\mathbf{r}}\left[\hat{\rho}(0)e^{i\hat{H}t/\hbar}|i\rangle\langle j|e^{-i\hat{H}t/\hbar}\right] \approx \sum_{ml}\int d\boldsymbol{\tau} G_0 G_0' [\hat{\rho}(0)^{\mathrm{W}}_{ml}] T_{mi} T'_{jl}, \tag{S7}$$

where $T_{mi} = \frac{1}{2}(q_i(t) + ip_i(t))(q_m(0) - ip_m(0))$ are the electronic transition amplitudes, $\int d\boldsymbol{\tau}$ represents the phase space integral with respect to all DOFs, and $(\hat{\rho}(0))^{ml}_{\mathrm{W}}$ is the partial Wigner transformations of operators $\hat{\rho}(0)$ with respect to the nuclear degrees of freedom $\{R, \mathbf{r}\}$. $G_0 = e^{-\frac{1}{2}\sum_m (q_m(0)^2 + p_m(0)^2)}$ provides the initial distributions of electronic degrees of freedom. The terms G_0' and T'_{jl} are similarly defined with respect to time propagation in the reversed direction.

Classical trajectories are used to evaluate the approximate time-dependent reduced density matrix in Eqn. S7. These trajectories are propagated using the equations of motion[4,8]

$$\dot{q}_i = \partial h/\partial p_i; \quad \dot{p}_i = -\partial h/\partial q_i; \quad F = -\frac{1}{2}\nabla_R \left[H(R,p,q) + H(R,p',q')\right], \tag{S8}$$

where $H(R,p,q) = \frac{1}{2}\sum_{ij} V_{ij}(R)\left(p_i p_j + q_i q_j\right)$ is the *classical* mapping Hamiltonian,[4] and F is the force that acts on the nuclear degrees of freedom.

With the PLDM approach, we numerically compute the light-matter diabatic population $\rho_{ii}(t)$ based on Eqn. S7, as well as the quantum yield of the isomerization reaction product (Trans configuration) as follows

$$Y = \lim_{t\to t_{\mathrm{P}}} \mathrm{Tr}_{\mathrm{R},\mathbf{r}} \left[\hat{\rho}(0) e^{i\hat{H}t/\hbar} h(R(t) - R_0) e^{-i\hat{H}t/\hbar}\right]. \tag{S9}$$

In the above equation, $h(R(t) - R_0)$ is the Heaviside function, $R_0 = -0.045$ a.u., which corresponds to both the maximum of $E_g(R)$ and the minimum of $E_e(R)$, is chosen to be the dividing surface of the reaction. Further, t_p is the plateau time of $P_I(t)$ when the population stop changing. For the model system investigated in this study, the plateau time is $t_p \approx 3 \sim 5$ ps. The quantum yield of the cis configuration is $1 - Y$.

Simulation details

The initial conditions for all simulations are $\hat{\rho}(0) = |\nu\rangle\langle\nu| \otimes \hat{\rho}_{\mathbf{n}}$, where the $|\nu\rangle$ indicates the initial electronic-photonic state, and $\hat{\rho}_{\mathbf{n}} = \hat{\rho}_R \otimes \hat{\rho}_{\mathbf{r}}$ represents the initial density operator for the nuclear DOF, with $\hat{\rho}_R$ for the reaction coordinate R and $\hat{\rho}_{\mathbf{r}}$ for the phonon modes $\mathbf{r}$. For Fig. 4, $|\nu\rangle$ is chosen to be the lowest polariton state, whereas for the rest of the simulation, $|\nu\rangle = |e,0\rangle$.

In Fig.1, to test the accuracy of the PLDM quantum dynamics simulation with numerically exact approach, we do not include the system-bath Hamiltonian $\hat{H}_{\mathrm{sb}}$, and set $T = 0$ K. The initial condition is $\hat{\rho}(0) = |\nu\rangle\langle\nu| \otimes \hat{\rho}_R$, where $\hat{\rho}_R = |\chi\rangle\langle\chi|$, where $\langle R|\chi\rangle =$

$\left(\frac{2\Gamma}{\pi}\right)^{1/4} e^{-(\Gamma/2)(R-R_0)^2}$ is a Gaussian wavepacket centered around $R_0 = 0.7$ a.u. with width $\Gamma = M\omega_R$, mass $M = 550$ Da, and frequency $\omega_R = 132.4$ cm^{-1}.

For calculations presented Fig. 2-5, $\hat{\rho}_{\mathbf{n}}$ is represented by the canonical thermal density, given by

$$\rho_{\mathbf{n}} = \mathrm{Tr}_{\mathbf{n}}[\hat{\rho}_{\mathbf{n}}] = \mathrm{Tr}_{R,\mathbf{r}}\left[e^{-\beta(\frac{\hat{P}^2}{2M}+\frac{M}{2}\omega_R^2(\hat{R}-R_0)^2)}e^{-\beta(\frac{\hat{\mathbf{p}}^2}{2m}+\frac{m}{2}\omega^2\hat{\mathbf{r}}^2)}\right]. \tag{S10}$$

For the reaction coordinate R, the mass is $M = 550$ Da, and frequency is $\omega_R = 132.4$ cm^{-1}, the thermal density of the reaction coordinate is centered around $R_0 = 0.7$ a.u. For the phonon bath modes, the mass is set to be $m = 1$ a.u. and the frequencies are sampled from the spectral density, with the details provided in the model Hamiltonian section. Further, $\beta = 1/k_{\mathrm{B}}T$, and the temperature is set to be $T = 300$ K for all of the results in Fig. 2-5. For PLDM simulations, the initial conditions for nuclear DOFs are generated from $[\hat{\rho}(0)^{\mathrm{W}}_{\gamma\mu}] = (\rho_{\mathbf{n}})^{\mathrm{W}}\delta_{\gamma\nu}\delta_{\mu\nu}$. For the Gaussian wavepacket used in Fig. 1, $[\hat{\rho}_R]^{\mathrm{W}} = \frac{1}{\pi}e^{-\Gamma(R-R_0)^2-(P-P_0)^2/\Gamma}$. For rest of the calculations, $[\rho_R]^{\mathrm{W}} = 2\tanh(\omega_R/k_{\mathrm{B}}T)e^{-\tanh(\omega_R/k_{\mathrm{B}}T)[M\omega_R(R-R_0)^2+P^2/M\omega_R]}$ for the reaction coordinate, and $[\rho_{\mathbf{r}}]^{\mathrm{W}} = \Pi_k 2\tanh(\omega_k/k_{\mathrm{B}}T)e^{-\tanh(\omega_k/k_{\mathrm{B}}T)[m\omega_k r_k^2+{p_k}^2/m\omega_k]}$, where ω_k is the frequency of the k_{th} bath mode, sampled from the spectral density $J(\omega)$ (with details provided in the model system section).

For the initial conditions of the mapping variables, we use the focused initial conditions,[9] $q_i = q_i' = \delta_{i\nu}$ and $p_i = -p_i' = \delta_{i\nu}$, to facilitate the numerical convergence. A total of 4×10^3 trajectories are used for all PLDM simulations.

Polariton Dynamics with various ω_c

Fig. S1 presents additional results of the polariton quantum dynamics for the model systems presented in Fig. 2 of the main text. The three columns corresponds to the results for the bare molecular system (panels a, d, g), hybrid molecule-cavity system with $\omega_c = 2.18$ eV (panels b, e, h), and with $\omega_c = 3.13$ eV (panels c, f, i). The results from three columns correspond to the schematics presented in Fig.2a-2c of the main text.

Fig. S1 a-c presents the time-dependent populations for the $|g,1\rangle$ (red) and $|e,0\rangle$ (blue) states. Fig. S1 d-f presents the time-dependent expectation value of the reaction coordinate $\langle R\rangle$. Fig. S1 g-i presents the time-dependent population of the trans configuration, defined in Eqn. 15 of the main text.

We emphasize that all of the non-adiabatic transitions (Fig. S1b-c) presented in this figure are induced by the quantum light-matter interactions $\hbar g_c$, as the model Hamiltonian in Eqn. S1 does not include the electronic non-adiabatic coupling (NAC) $\langle e|\nabla|g\rangle$. The effect of the electronic NAC on the quantum yield will be investigated in the following section.

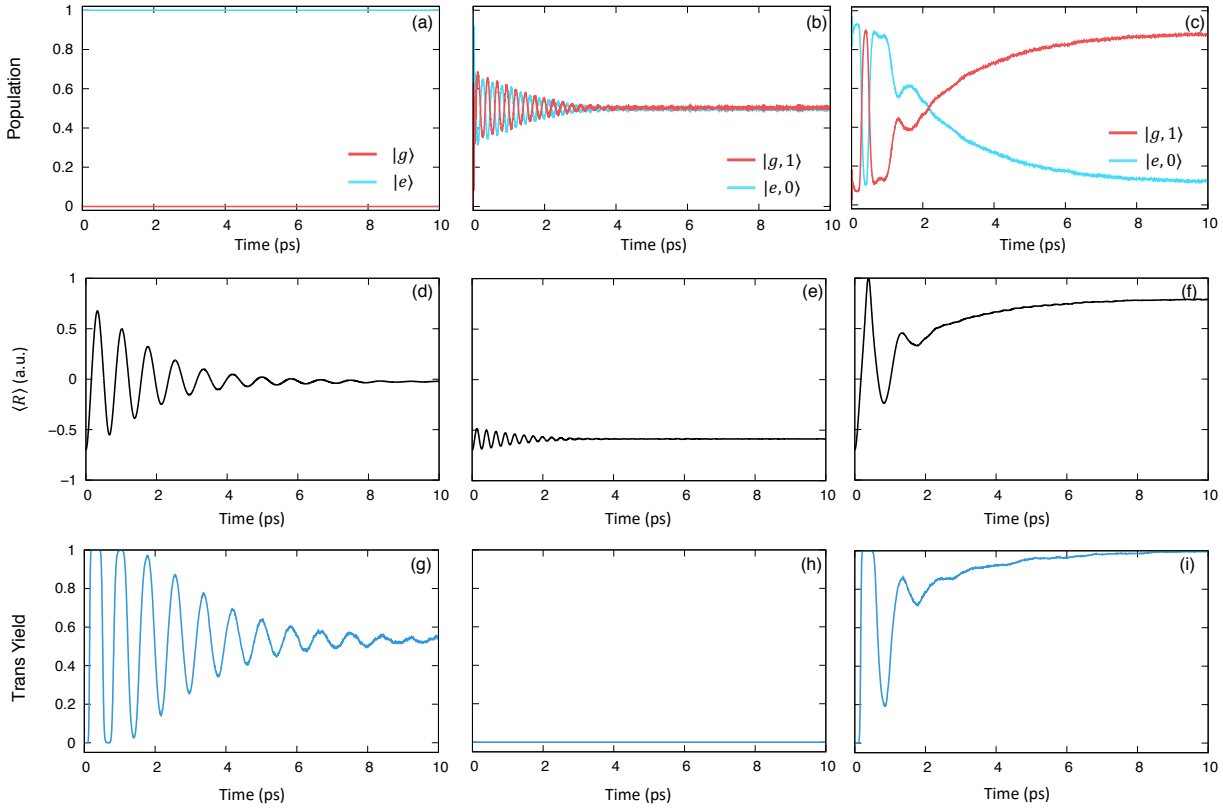

Figure S1: Population dynamics for (a) the bare molecular system, (b) hybrid molecule-cavity system with $\omega_c = 2.18$ eV, and (c) with $\omega_c = 3.13$ eV. Time-dependent expectation of the nuclear coordinate R are provided in panels d-f. Time-dependent yield of the Trans isomer are provided in panels g-i.

Polariton dynamics with the electronic non-adiabatic coupling

In the main text, we have set the derivative coupling $\langle g(R)|\nabla_R|e(R)\rangle = 0$, in order to clearly demonstrate the new chemical reactivities induced by quantum light-matter interactions. Here, we demonstrate that the presence of the electronic non-adiabatic coupling (NAC) does not qualitatively (or even semi-quantitatively) change the results presented in this study.

To this end, we generalize the Hamiltonian in Eqn. S1 to include the non-adiabatic couplings as follows

$$\hat{H}_e = \hat{T}_R + \sum_{i,j=\{g,e\}} \hat{d}_{ij}|i(R)\rangle\langle j(R)| + E_g(R)|g(R)\rangle\langle g(R)| + E_e(R)|e(R)\rangle\langle e(R)|, \tag{S11}$$

where $\hat{d}_{ij} = -\frac{\hbar}{M}\langle i(R)|\nabla_R|j(R)\rangle\nabla_R - \frac{1}{2M}\langle i(R)|\nabla_R^2|j(R)\rangle$. We model the derivative coupling with the following Lorentzian function

$$\langle e(R)|\nabla_R|g(R)\rangle = \frac{1}{2}\frac{G}{G^2 + (R-R_0)^2}, \tag{S12}$$

where G is a parameter that describes the strength of the derivative coupling. The second derivative coupling $\langle i(R)|\nabla_R^2|j(R)\rangle/2M$ is directly related to the derivative coupling, which will be obtained after introducing the mixing angle in Eqn. S15.

Two diabatic states, $|a\rangle$ and $|b\rangle$, can be constructed through an unitary rotation of the adiabatic states $|e\rangle$ and $|g\rangle$ with a mixing angle $\theta(R)$ as follows

$$\begin{aligned} |g(R)\rangle &= \cos\theta(R)|a\rangle + \sin\theta(R)|b\rangle \\ |e(R)\rangle &= -\sin\theta(R)|a\rangle + \cos\theta(R)|b\rangle \end{aligned} \tag{S13}$$

Note that $\theta(R)$ is the mixing angle between diabatic states in a bare molecular Hamiltonian $\hat{H}_e$, which is different than the mixing angle ϕ between photon-dressed states introduced in the main text.

The derivative coupling is related to the mixing angle through the following relation

$$\begin{aligned}\langle e(R)|\nabla_R|g(R)\rangle &= \Big[-\sin\theta(R)\langle a| + \cos\theta(R)\langle b|\Big]\cdot\nabla_R\Big[\cos\theta(R)|a\rangle + \sin(\theta(R))|b\rangle\Big] \\ &= \Big[-\sin\theta(R)\langle a| + \cos\theta(R)\langle b|\Big]\cdot\Big[-\sin\theta(R)|a\rangle + \cos\theta(R)|b\rangle\Big]\nabla_R\theta(R) \\ &= \nabla_R\theta(R).\end{aligned} \tag{S14}$$

The mixing angle is thus obtained from integrating the derivative coupling in Eqn. S12, with a proper choice of reference angle ($\theta_0 = \pi/4$) as follows

$$\theta(R) = \int\langle e|\nabla_R|g\rangle dR + \theta_0 = \frac{1}{2}\tan^{-1}\big(\frac{R-R_0}{G}\big) + \frac{\pi}{4}. \tag{S15}$$

The second derivative coupling (in Eqn. S11), on the other hand, can be shown to obey $\langle g(R)|\nabla_R^2|g(R)\rangle = \langle e(R)|\nabla_R^2|e(R)\rangle = -(\nabla_R\theta(R))^2$, thus is also available with the expression of $\theta(R)$ in Eq. S15.

The electronic Hamiltonian $\hat{H}_{\rm e}$ in Eqn. S11 under the diabatic representation $\{|a\rangle, |b\rangle\}$ is

$$\hat{H}_{\rm dia} = \hat{T}_R + V_{aa}(R)|a\rangle\langle a| + V_{bb}(R)|b\rangle\langle b| + V_{ab}(R)\Big(|a\rangle\langle b| + |b\rangle\langle a|\Big) \tag{S16}$$

where the matrix elements are obtained by applying the unitary transformation (Eqn. S13) on the adiabatic potentials, resulting in the following expressions for the diabatic potentials and coupling

$$\begin{aligned}V_{aa}(R) &= E_g(R)\cos^2\theta(R) + E_e(R)\sin^2\theta(R) \\ V_{bb}(R) &= E_g(R)\sin^2\theta(R) + E_e(R)\cos^2\theta(R) \\ V_{ab}(R) &= \Big(E_g(R) - E_e(R)\Big)\sin\theta(R)\cos\theta(R).\end{aligned} \tag{S17}$$

Here, $E_g(R)$ and $E_e(R)$ are defined in Eqn. S2, and $\theta(R)$ is defined in Eqn. S15. The

adiabatic potential, of course, are the eigenvalue of the diabatic potential matrix, with the familiar expression $\frac{1}{2}(V_{aa}+V_{bb}) \pm \frac{1}{2}\sqrt{(V_{aa}-V_{bb})^2+4V_{ab}^2}$ that returns back to the $E_g(R)$ and $E_e(R)$ expressions. The mixing angle, on the other hand, can be expressed with diabatic couplings through $\theta = \frac{1}{2}\tan^{-1}[2V_{ab}/(V_{aa}-V_{bb})]$. These relationship can be easily verified with the diabatic potentials and couplings in Eqn. S17. It is also easy to verify that in the diabatic representation, the derivative coupling terms $\sum_{ij}\hat{d}_{ij}|i(R)\rangle\langle j(R)|$ in Eqn. S11 completely vanish, as one expects.

The value of G depends on the particular system of interest. For diatomic systems like NaI, LiF etc. the NAC can be described by a Lorentzian shape with a peak value in the range of 1$\sim$ 5 a.u.[10,11] In organic molecules like azobenzene or stillbene, the ensemble average of the absolute value of the NAC lie between 2$\sim$6 a.u.[12] Here, the peak of the NAC, given by $\frac{1}{2G}$ has been varied from 50 to 0.05. However, we want to emphasize that the peak value of NAC is not the only quantity that controls the non-adiabatic dynamics. In our model, the relatively large energy gap between the ground and excited electronic states effectively suppress the non-adiabatic transitions between $|g,0\rangle$ and $|e,0\rangle$, and the presence of the NAC does not qualitatively or semi-quantitatively change any result presented in the main text. The results presented below corresponds to a NAC peak of 5 a.u. (G=0.1 a.u.).

All of the PLDM quantum dynamics simulations are performed with the diabatic Hamiltonian in Eqn. S16.

Fig. S2a presents the non-adiabatic coupling with $G = 0.1$ a.u. (violet dotted line), the adiabatic potentials $E_g(R)$ (black solid line) and $E_e(R)$ (blue solid line), and the diabatic potentials $V_{aa}(R)$ (red dotted line) and $V_{bb}(R)$ (yellow dotted lines). In the isolated molecule the non-adiabatic coupling induces transitions between $|g\rangle$ and $|e\rangle$. With the presence of the cavity, this derivative coupling will only induce the transitions between $|g,0\rangle$ and $|e,0\rangle$ states, or between $|g,1\rangle$ and $|e,1\rangle$ states. It will not couple $|g,1\rangle$ and $|e,0\rangle$ states which play the most important role in polariton photochemical processes investigated in this study. This is because that $|g,1\rangle$ and $|e,0\rangle$ states differ by 1 photon, thus $\langle g,1|\nabla_R|e,0\rangle = \langle g|\nabla_R|e\rangle \cdot \langle 1|0\rangle =$

0, due to the orthogonality the Fock states. Fig. S2b and Fig. S2c present the yield of the isomerization reaction by varying $\hbar\omega_c$ and $\hbar g_c$, respectively. In both cases, the presence of the electronic non-adiabatic coupling does not qualitatively (or even semi-quantitatively) change the results presented in the main text. Thus, even with the presence of the non-adiabatic coupling, the control schemes presented in the main text remains the same.

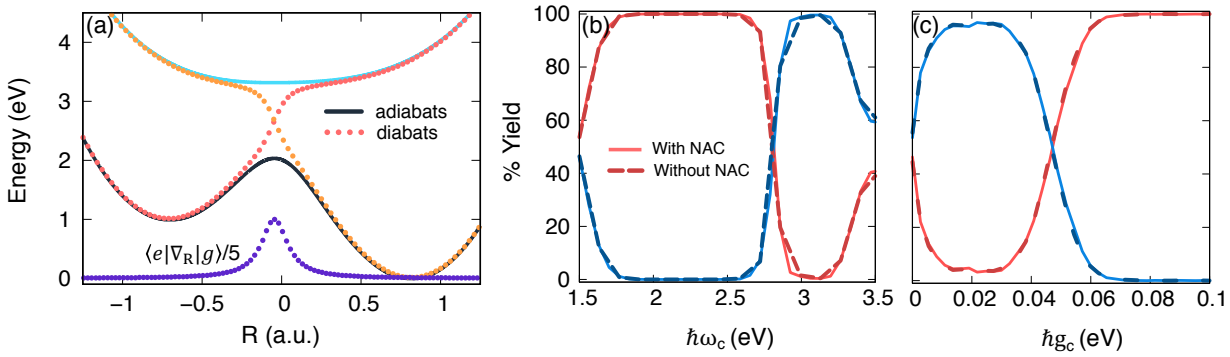

Figure S2: The isomerization model system in the presence of non-adiabatic coupling. (a) The non-adiabatic coupling (violet dotted line), diabatic potentials (yellow and red dotted lines), and adiabatic potentials (blue and black solid lines). (b) The yield of the cis (red) and trans (blue) isomer at various photon frequency $\hbar\omega_c$, with and without the presence of the non-adiabatic coupling (NAC); the rest parameters are the same as in Fig. 2 of the main text. (c) The yield of cis (red) and trans (blue) isomer at various coupling strength $\hbar g_c$; the rest parameters are the same as in Fig. 3 of the main text.

Polariton dynamics with a position-dependent transition dipole

Here, we test the effect of the position-dependent transition dipole moment on polariton quantum dynamics. Following the previous work[13] on polariton photo-isomerization, we model the light-matter interaction with the following expression

$$\hbar g_c(R) \equiv \boldsymbol{\mu}_{\mathrm{eg}}(R) \cdot \hat{\mathbf{e}} \sqrt{\frac{\hbar\omega_c}{2V_c\epsilon_0}} = \frac{2}{\pi} \tan^{-1}\left(\frac{R-R_0}{G}\right) \cdot \hbar g_c^0 \tag{S18}$$

where $\hbar g_c^0$ is the constant value used in the main text. We also assume that the transition dipole will change in the same range as the non-adiabatic coupling (by using the same parameter G in the above expression). Thus, the asymptotic value of this function is $\pm\hbar g_c^0$.

With this new position-dependent light-matter interaction, $\hbar g_c(R)$, we investigate the quantum yield of isomerization by changing the photon frequency $\hbar\omega_c$ and the asymptotic value of the light-matter interaction $\hbar g_c^0$. Here, we will use the model system that contains the non-adiabatic coupling presented in the previous section. We further compare these results to those presented in the main text, *i.e.*, without NAC and with a constant $\hbar g_c^0$. The results with NAC and a constant coupling strength $\hbar g_c^0$ are provided in Fig. S2.

Fig. S3a presents the position-dependent coupling $\hbar g_c(R)$ that significantly change its character in the region of NAC (see Fig. S2a). This position-dependent coupling, however, only slightly modify the numerical results of the quantum yield compared to the constant coupling model, and does not qualitatively change the behavior of the control scheme when changing the photon frequency in (b) or the asymptotic coupling strength $\hbar g_c^0$ in (c).

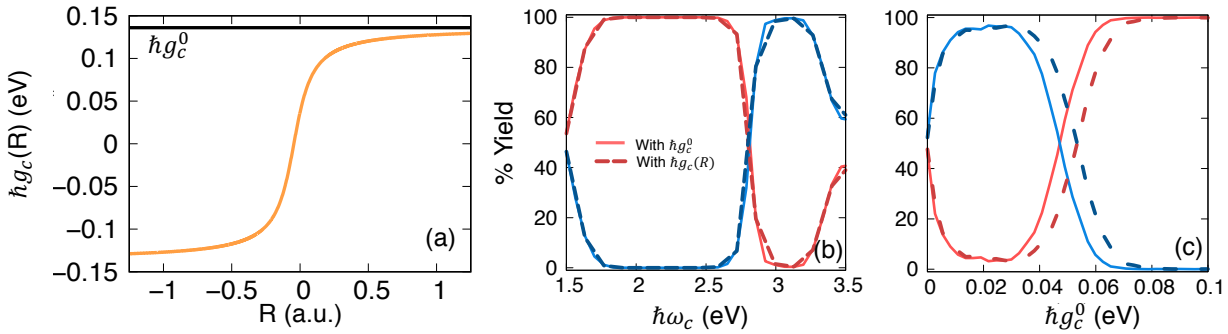

Figure S3: (a) The position-dependent light-matter coupling strength $\hbar g_c(R)$. (b) Yield of cis (red) and trans (blue) isomer at various photon frequency $\hbar\omega_c$, with NAC and using $\hbar g_c(R)$ (solid) and without NAC and using $\hbar g_c^0$. The rest parameters are the same as in Fig. 2 of the main text. (c) The Yield of cis (red) and trans (blue) isomer at various asymptotic coupling strength $\hbar g_c^0$; the rest parameters are the same as in Fig. 3 of the main text.

References

(1) Galego, J.; Garcia-Vidal, F. J.; Feist, J. Many-Molecule Reaction Triggered by a Single Photon in Polaritonic Chemistry. *Phys. Rev. Lett.* **2017**, *119*, 136001.

(2) Makri, N. The Linear Response Approximation and its Lowest Order Corrections: An Influence Functional Approach. *J. Phys. Chem. B* **1999**, *103*, 2823–2829.

(3) Walters, P. L.; Allen, T. C.; Makri, N. Direct determination of discrete harmonic bath parameters from molecular dynamics simulations. *J. Comput. Chem.* **2017**, *38*, 110–115.

(4) Huo, P.; Coker, D. F. Communication: Partial Linearized Density Matrix Dynamics for Dissipative, Non-Adiabatic Quantum Evolution. *J. Chem. Phys.* **2011**, *135*, 201101.

(5) Meyer, H.; Miller, W. H. A Classical Analog for Electronic Degrees of Freedom in Nonadiabatic Collision Processes. *J. Chem. Phys.* **1979**, *70*, 3214–3223.

(6) Stock, G.; Thoss, M. Semiclassical Description of Nonadiabatic Quantum Dynamics. *Phys. Rev. Lett.* **1997**, *78*, 578–581.

(7) Thoss, M.; Stock, G. Mapping Approach to the Semiclassical Description of Nonadiabatic Quantum Dynamics. *Phys. Rev. A* **1999**, *59*, 64–79.

(8) Lee, M. K.; Huo, P.; Coker, D. F. Semiclassical Path Integral Dynamics: Photosynthetic Energy Transfer with Realistic Environment Interactions. *Annu. Rev. Phys. Chem.* **2016**, *67*, 639–668.

(9) Bonella, S.; Coker, D. F. Semiclassical Implementation of the Mapping Hamiltonian Approach for Nonadiabatic Dynamics using Focused Initial Distribution Sampling. *J. Chem. Phys.* **2003**, *118*, 4370–4385.

(10) Giese, T. J.; York, D. M. Complete basis set extrapolated potential energy, dipole, and polarizability surfaces of alkali halide ion-neutral weakly avoided crossings with and without applied electric fields. *J. Chem. Phys.* **2004**, *120*, 7939–7948.

(11) Kowalewski, M.; Bennett, K.; Mukamel, S. Cavity Femtochemistry: Manipulating Nonadiabatic Dynamics at Avoided Crossings. *J. Phys. Chem. Lett.* **2016**, *7*, 2050–2054.

(12) Neukirch, A. J.; Shamberger, L. C.; Abad, E.; Haycock, B. J.; Wang, H.; Ortega, J.; Prezhdo, O. V.; Lewis, J. P. Nonadiabatic Ensemble Simulations of cis-Stilbene and cis-Azobenzene Photoisomerization. *J. Chem. Theory Comput.* **2014**, *10*, 14–23.

(13) Galego, J.; Garcia-Vidal, F. J.; Feist, J. Suppressing photochemical reactions with quantized light fields. *Nat. Commun.* **2016**, *7*, 13841 EP.